Proxy-based sliding-mode tracking control of dielectric elastomer actuators through eliminating rate-dependent viscoelasticity

Jiang Zou[1], James D. J. MacLean[2], Jieji Ren[1], Sumeet S. Aphale[2] & Guoying Gu[1*]

[1]The State Key Laboratory of Mechanical System and Vibration and the Robotics Institute, School of Mechanical Engineering, Shanghai Jiao Tong University, Shanghai 200240, China.

[2]The Artificial Intelligence, Robotics and Mechatronic Systems (ARMS) Group, School of Engineering, University of Aberdeen, Aberdeen, UK.

E-mail: guguoying@sjtu.edu.cn

June 2022

Abstract. Dielectric elastomer actuators (DEAs) usually suffer from rate-dependent viscoelastic nonlinearity, which manifests as hysteresis in their deformation cycles, leading to huge challenges in their modeling and control. In this work, we propose a model-free, proxy-based, sliding-mode tracking control approach to mitigate viscoelastic nonlinearity, achieving high-precision tracking control of DEAs. To this end, we first investigate the viscoelastic nonlinearity of DEAs, revealing its asymmetric and rate-dependent characteristics. Then, by combining the benefits of the PID control for small positioning errors and sliding-mode control for large errors, a proxy-based, sliding-mode tracking controller (PBSMC) is established. Finally, the stability of the controller is analyzed. To verify the effectiveness of the controller, several experiments are conducted to demonstrate the performance of DEAs in tracking sinusoidal trajectories under different frequencies. The experimental results demonstrate that with the PBSMC, the DEA can precisely track sinusoidal trajectories within a frequency range of 0.1 Hz to 4.0 Hz by effectively minimizing the effect of inherent viscoelastic nonlinearity. Compared with open-loop tracking performance, the proxy-based, sliding-mode controlled DEA performance shows a significant reduction in maximum tracking error from 45.87% to 8.72% and in root-mean-square (RMS) error from 24.46% to 3.88%. The main advantages of the proxy-based, sliding-mode control are: i) it adopts a model-free approach, avoiding the need for complex dynamic modeling; ii) it can achieve high-precision tracking control of DEAs, thereby paving the way for the adoption of DEAs in several emerging applications.

1. Introduction

Dielectric elastomer actuators (DEAs) have shown huge potential applications in the field of soft robotics, owing to their large deformation, high energy density and fast

response characteristic [1, 2]. In general, DEAs mainly consist of a dielectric elastomer membrane coated with compliant electrodes with special pattern. When a high voltage is applied, the electrostatic force between the electrodes leads to an expansion in the area and a decrease in the thickness of DEAs [3, 4]. Based on this working principle, DEAs with different configurations have been developed to generate various actuations, such as elongation, bending, twisting, contraction and so on [5, 6]. During the last two decades, several exciting applications of DEA-based soft robots have been reported, such as climbing robots [7], swimming robots [8], flying robots [9], gripping robots [10], crawling robots [11, 12] and wearable robots [13], showcasing the remarkable advantage of DEAs in term of mimicking biological movements and functions. To further advance the adoption of DEAs in future applications, a significant improvement in their tracking performance has been highlighted as being extremely desirable. However, due to their inherent viscoelastic nonlinearity, the dynamic responses of DEAs usually suffer from complex nonlinear dynamics, including creep and hysteresis nonlinearity [14]. Of the two, hysteresis is an asymmetric and rate-dependent nonlinearity that presents a huge challenge in the dynamic modeling of DEAs and also, severely limits the actuator's trajectory tracking precision [15].

In general, viscoelastic nonlinearity is described as a type of dissipative phenomenon [16]. Based on the non-equilibrium thermodynamics theory, a general framework to describe dynamic responses of DEAs including viscoelastic nonlinearity has been proposed in [17]. According to the framework, number of physical models have been proposed for DEAs. However, most of those models are too complicated to be adopted for any applicable control design [18]. Different from physical models, some phenomenological models (such as rate-dependent or rate-independent Prandtl-Ishlinskii model) have also been introduced for DEAs. These models are based on the experimentally measured actuator responses and dont take into account the physical properties dimensions of DEAs. The main advantage of the phenomenological models is that they can be used to eliminate the viscoelastic nonlinearity by applying direct inverse hysteresis compensation approaches [19, 15, 20]. However, these models usually are effective within a specific frequency range and require a complex parameter identification process, thereby limiting their wide applications. Simplified models that overcome the complex geometric shapes of the DEAs by formulating the DEA dynamics as a combination of a 1-DOF mass-spring-damper system combined with suitable rheological dynamics, have also been developed in [21, 22, 23]. Based on these simplified dynamic models, nonlinear controllers, such as nonlinear PID [24], adaptive sliding mode controller [25, 26], a cerebellum model articulation nonlinear controller [27], etc, have been proposed to remove the nonlinearity of DEAs. However, their performance is limited to viscoelastic compensation at a single frequency or for small deformations. Therefore, it is still lack of effective approach to quantitatively describe the rate-dependent viscoelastic responses of DEAs. However, most of existed control approaches usually rely on the dynamic models, increasing the difficulty to eliminate such kinds of nonlinearity. A model-free tracking control provide a strategy to overcome

the drawback of existed control approaches, but is still not achieved for mitigating the rate-dependent viscoelastic nonlinearity of DEAs.

In [28, 29, 30], the PBSMC has been proposed. It is a model-free approach that combines the error suppression benefits of the PID control with the fast, responsive nature of the sliding mode control (SMC), thereby demonstrating the potential to be adaptable of eliminating the viscoelastic nonlinearity (hysteresis) in DEAs. This work starts by analyzing the experimentally recorded dynamic responses of the DEA and characterizing the inherent rate-dependent viscoelastic nonlinearity (hysteresis). In an attempt to demonstrate the effectiveness of a model-free control approach (the first such endeavor to the best of our knowledge), the PBSMC is designed, simulated and experimentally validated on the DEA. A full stability analysis of the closed-loop system is also presented. Sinusoidal as well as triangular trajectories are used as reference. Tracking errors are quantified. It is shown that the designed controller is capable of accurately tracking sinusoids within a frequency range of 0.1 Hz and 4.0 Hz with RMS errors as low as 3.88%. It is further shown that complex, broad-spectrum trajectories such as triangular trajectories in the range of 0.08 Hz to 0.8 Hz can also be tracked accurately with RMS errors as low as 1.59%. This rigorous validation of a model-free control scheme opens up a wide range of applications for the DEAs.

The main advantages of the PBSMC for DEAs depend on the facts that:

i) The PBSMC is one kind of model-free control approaches. Although lots of models (physical-based or phenomenological based) have been developed to describe the viscoelastic responses of DEAs, they usually are difficult to be converted into control model or limited to special frequency range. Hence, the PBSMC avoids the challenge on dynamic modeling in DEAs.

ii) The stability of the PBSMC is proved for DEAs. As it is the first time to employ the PBSMC to remove the rate-dependent viscoelastic nonlinearity in DEA, its stability is analytically proved by combining with a dynamic model, which pave the way for further application in the field of DEAs.

iii) With the PBSMC, DEAs can achieve high-precision tracking control. Different from existed control approaches, which mainly are valid for tracking static trajectories or effective for specifical frequency, the PBSMC can eliminate the rate-dependent viscoelastic nonlinearity in DEAs.

The remainder of this work is organized as follows. Section II introduces the planar DEAs, the experimental setup and the features of their dynamic responses. Section III presents the design and stability analysis of the PBSMC. Section IV shows the experimental results demonstrating the effectiveness of the designed controller. Section V concludes this paper.

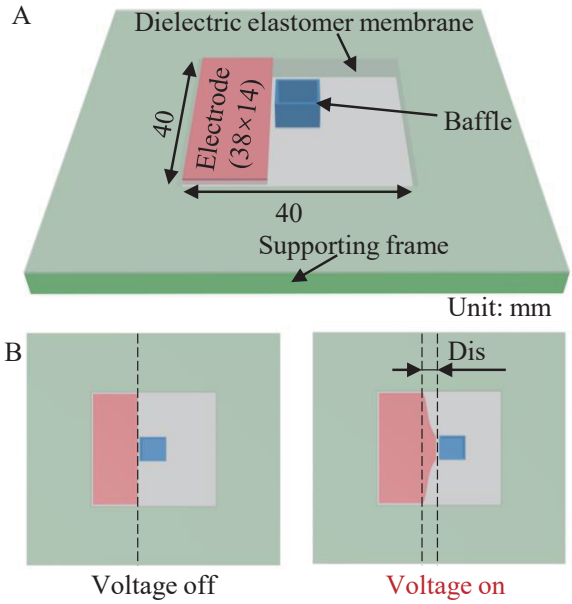

Figure 1. A) A simplified planar view of the geometric structure of the planar DEA; B) A graphical representation of the planar DEA deformation when excitation voltage is applied.

2. System description

2.1. Actuator fabrication

In this section, a planar DEA with one degree-of-freedom is designed and fabricated for proof-of-concept testing. Fig. 1A shows the structure and geometric size of the planar DEA. It mainly contains a single layer of dielectric elastomer membrane (Wacker ELASTOSIL Film 2030, undeformed thickness 0.1 mm) with an equiaxial pre-stretch ratio of 1.5. A stiff frame made of a laser-cut polymethyl methacrylate (PMMA) board (thickness 3 mm) is adopted to support the pre-stretched silicone membrane. The silicone membrane is separated into two regions: passive region and active region. In the active region, carbon grease (MG Chemical 846-80G) working as compliant electrodes is used to coat both sides (There is an interval of 1 mm between the electrodes and the edges of the active region to avoid the electric breakdown). The passive region is utilized as a nonlinear spring. A baffle is adhered to the middle of the silicone membrane, providing convenience for displacement measurement. The working principle of the planar DEA is shown in Fig. 1B. When a high voltage is applied to the electrodes, the static force between the electrodes squeezes the active region, leading to expand of the active region and shrink of the passive region. As a result, the baffle generates an output displacement. The breakdown voltage for the DEA employed in the experiments is approximately 4.5 kV and consequently, the exciting voltage applied during the experiments is kept below 4.0 kV.

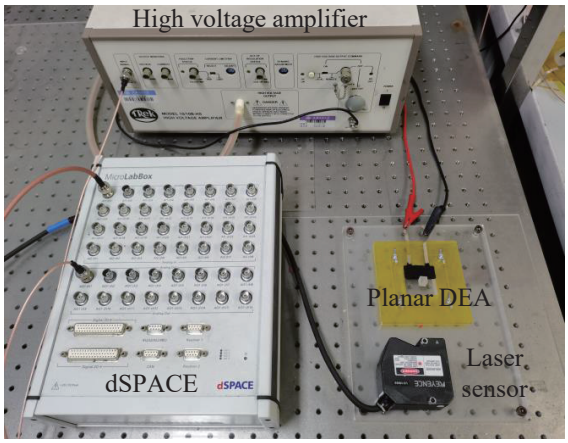

Figure 2. The layout of the experimental setup clearly showing the planar DEA, the laser-based displacement sensor, the high-voltage amplifier used to supply excitation voltage and the dSPACE Microlab box used as the control interface.

2.2. Experimental setup

Fig. 2 shows the experimental platform utilized to investigate the viscoelastic nonlinearity of the planar DEA and verify the effectiveness of our control approach. It mainly consists of a high voltage amplifier (Trek 10/10B-HS), a laser sensor (Keyence LK-H085), a control module (dSPACE Microlab 1020) and a planar DEA. The high voltage amplifier with a gain of 1000 is used to generate exciting voltage for the planar DEA. The laser sensor is used to capture the output displacement and convert the displacement (in the range of -20 mm to 20 mm) into analog signal (in the range of -10 V to 10 V). The control module with 16-bit analog-to-digital converter and 16-bit digital-to-analog converter is used to generate control signal for the high voltage amplifier and record the displacement from the laser sensor. The sampling time is set as 0.1 ms in this work.

2.3. Open-loop dynamics

Based on the experimental platform, we investigate the dynamic responses of the planar DEAs to reveal its rate-dependent viscoelastic nonlinearity. We should mention that the bandwidth of the planar DEAs generally is limited to several Hz [31]. Considering this is the early attempt to develop PBSMC for DEAs, the maximum working frequency of the planar DEA is selected as 4.0 Hz. The experimental results are illustrated in Fig. 3. Fig. 3A shows one example of the output displacement when the frequency equals to 1.0 Hz. It is evident from Fig 3A that the dynamic response of the planar DEA shows a slow drift in position for the first few cycles and then settles down (an effect of the intrinsic creep nonlinearity) [15, 19]. In Figure 3B, one cycle of the periodic displacement trajectory after creep is plotted as a function of the exciting voltage at 0.1 Hz, 0.5 Hz, 1.0 Hz and 4.0 Hz, respectively. It can be observed that as the hysteresis nonlinearity of the planar DEA usually is asymmetric and rate-dependent [14, 16, 17], the width of

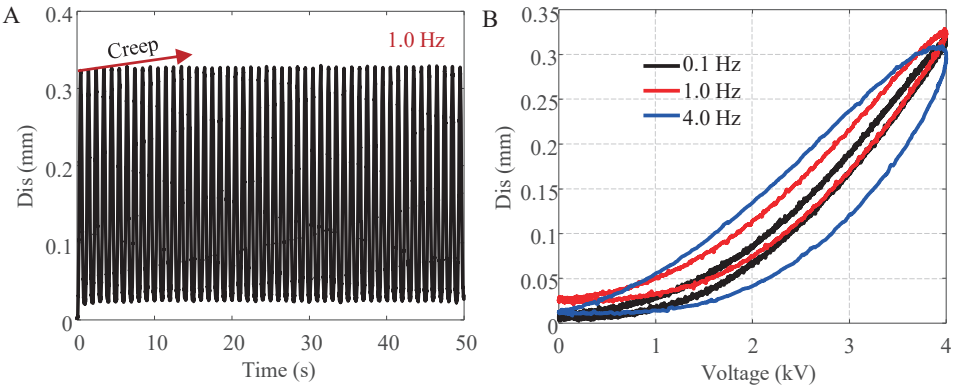

Figure 3. The dynamic responses of the planar DEA. A) Creep nonlinearity; B) Rate-dependent hysteresis nonlinearity.

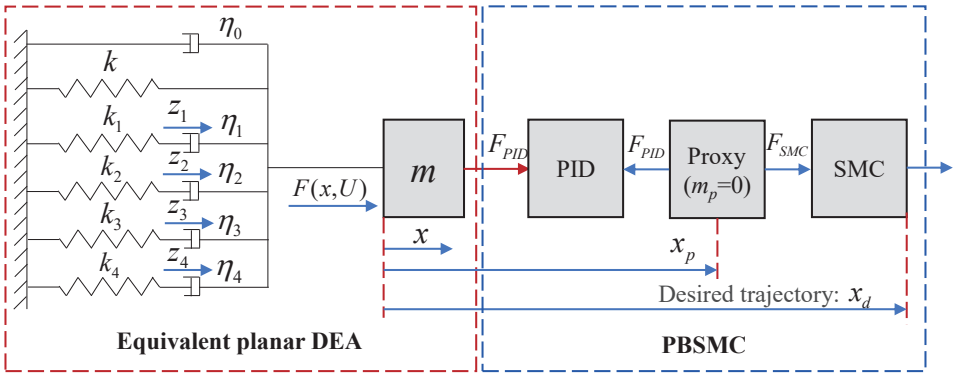

Figure 4. Block-diagram representing the working principle of the PBSMC.

the hysteresis loops rapidly increases with increase in frequency of the exciting voltages. As we discussed above, existed control methods usually fail to remove such kind of nonlinearity of DEAs. In addition, they belong to model-based approaches, increasing the difficulty for controller design. To overcome the drawback of existed control methods, this work is motivated to develop a model-free control approach to remove the rate-dependent viscoelastic nonlinearity of DEAs, achieving high-precision tracking control. To this end, a PBSMC for the planar DEA is designed and its stability is also proved. Further, different tracking experiments are conducted to verify the effectiveness of the controller.

3. Design of the PBSMC

In this section, the PBSMC is designed. To perform simulations and ascertain closed-loop stability, a dynamic model for the DEA is then established. Note that the control design is independent of the established DEA model. The model is only used to ascertain closed-loop performance in simulations and further prove closed-loop stability.

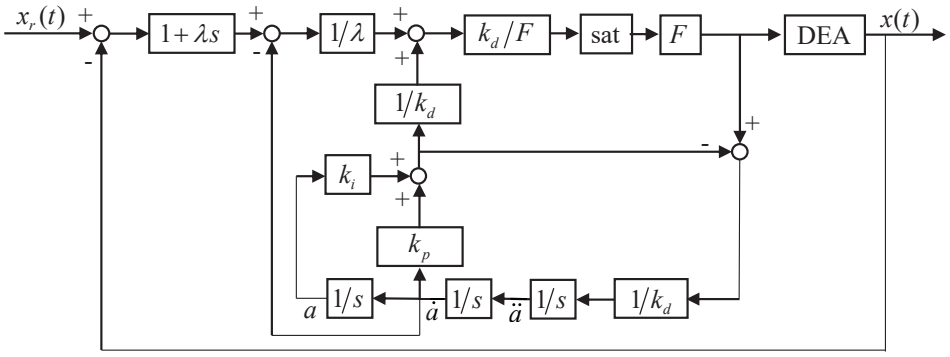

Figure 5. The equivalent block-diagram of the PBSMC.

3.1. Working principle of the PBSMC

Fig. 4 shows the working principle of the PBSMC. We should mention that: for the convenience of description, the planar DEA is equivalent to a single degree-of-freedom spring-damping-mass system combining with a few rheological models (See the next subsection for the detail of the equivalent system). The key of the PBSMC depends on the fact that a virtual object, referred as a proxy, is introduced into the control system [29, 30]. The proxy mass side of the controller is controlled by extended sliding-mode controller which quickly reaches the user defined manifold of interest. As this happens, the PID control portion follows where the proxys manifold is and eliminates the error between the proxys manifold and the actual position of the planar DEA. Once the control system is reduced to only small position errors, PBSMC behaves like an extended PID control in this instance eliminating small position errors with great effect. As a result, the planar DEA can achieve high-precision tracking control. As shown in Fig. 4, the interaction force of the PID controller and the SMC are defined as F_{PID} and F_{SMC}, respectively. The position of the planar DEA, the proxy and the desired trajectory are defined as x, x_p and x_d, respectively. Their corresponding speeds are $\dot{x}_p$ and $\dot{x}_d$, respectively. The SMC law is defined as:

$$F_{SMC} = F\mathrm{sgn}\left(\sigma_1\right), \tag{1}$$

where $\sigma_1 = x_d - x_p + \lambda\left(\dot{x}_d - \dot{x}_p\right)$ is the sliding surface. *sgn* represents the signum function. The F and λ are two positive gains. Based on the sliding surface, it can be seen that when proxy is within the sliding surface, the error dynamics is determined by:

$$\sigma_1 = x_d - x_p + \lambda\left(\dot{x}_d - \dot{x}_p\right) = 0. \tag{2}$$

Therefore $x_d - x_p = \rho e^{-t/\lambda}$, where ρ is a constant ratio. It can be seen that the position error and velocity error of the proxy will exponentially decay to zero with a time constant λ. As a result, the proxy can track the desired trajectory.

The F_{PID} can be described as:

$$F_{PID} = k_p \left(x_p - x\right) + k_i \int_0^t \left(x_p - x\right) d\tau + k_d \left(\dot{x}_p - \dot{x}\right), \tag{3}$$

where k_p, k_i and k_d represent three constant gains of the PID controller. Further, we define:

$$a = \int_0^t \left(x_p - x\right) d\tau, \tag{4}$$

and

$$\sigma = x_d - x + \lambda \left(\dot{x}_d - \dot{x}\right). \tag{5}$$

Then, (2) can be rewritten as:

$$\sigma_1 = \sigma - \dot{a} - \lambda \ddot{a}. \tag{6}$$

which results in

$$F_{SMC} = F\mathrm{sgn}(\sigma - \dot{a} - \lambda \ddot{a}), \tag{7}$$

and

$$F_{PID} = k_p \dot{a} + k_i a + k_d \ddot{a}. \tag{8}$$

According to the force analysis of the proxy, the following holds

$$m_p \ddot{x}_p = F_{SMC} - F_{PID}. \tag{9}$$

Further, by setting the m_p as zero:

$$F_{SMC} = F_{PID} = f, \tag{10}$$

therefore, the proxy-based sliding-mode tracking control law is obtained by

$$f = k_p \dot{a} + k_i a + k_d \ddot{a} = F\mathrm{sgn}(\sigma - \dot{a} - \lambda \ddot{a}). \tag{11}$$

Thus, $\ddot{a}$ can be solved as [30]:

$$\ddot{a} = -\frac{k_p \dot{a} + k_i a}{k_d} + \frac{F}{k_d} sat\left[\frac{k_d}{F}\left(\frac{\sigma - \dot{a}}{\lambda} + \frac{k_p \dot{a} + k_i a}{k_d}\right)\right], \tag{12}$$

where *sat* represents the saturation function. Thus, (11) can be rewritten as:

$$f = F sat\left[\frac{k_d}{F}\left(\frac{\sigma - \dot{a}}{\lambda} + \frac{k_p \dot{a} + k_i a}{k_d}\right)\right]. \tag{13}$$

Based on (11-13), the block-diagram in Fig. 4 can be further equivalent to a new block-diagram in Fig. 5. To employ the PBSMC, its stability must first be proven.

3.2. Dynamic modeling

To prove the stability of the PBSMC, a proper dynamic model is necessary. We should mention that the PBSMC is one kind of model-free control approach. The dynamic model is only applied to prove its stability. To describe the dynamic responses of the planar DEA, it is required to simplify its non-uniform deformation because it is very difficult to take every point into consideration. Therefore, the planar DEA is approximated to be that of a one-degree-of-freedom spring-damping-mass system, as shown in Fig. 4. The spring stiffness k represents the stretch force caused by the deformation of the dielectric elastomer membrane. η_0 is the damping ration due to the air drags. m is the equivalent mass of the planar DEA. When a high voltage U is applied, the DEA generates an actuation force $F(x, U)$. Based on the working principle of the DEA, it is assumed that

$$F\left(x, U\right) = U^2(bx^2 + cx + d), \tag{14}$$

where b, c and d represent three constant ratios. Thus, the dynamic model of the planar DEA can be expressed as:

$$\begin{aligned} m\ddot{x} &= -kx - \sum_{i=1}^{4} k_i z_i + F\left(x, U\right) - \eta_0 \dot{x}, \\ k_i z_i &= \eta_i(\dot{x} - \dot{z}_i), \end{aligned} \tag{15}$$

where k_i and η_i represent the stiffness and damping ratio of each rheological model. And i equals to 1, 2, 3 and 4, respectively. In (15), there are 14 unknown parameter that need to be identified based on the experimental data. To this end, we first need to define a loss function. Based on the trial-and-error method, we select a loss function to balance the predicted errors for different frequencies. The loss function can be expressed as::

$$J_\theta = \omega_1 \times \frac{1}{n} \sum_{i=1}^{3} \left(y_{ia} - y_{ir}\right)^2 + \omega_2 \times \max\left([y_{1a} - y_{1r}, y_{2a} - y_{2r}, y_{3a} - y_{3r}]\right) \tag{16}$$

where ω_1 and ω_2 represent two positive constants. y_{ia} and y_{ir} are the ith experimental data and predicted results, respectively. n represents the length of the experimental data. θ represents the 14 unknown parameters. Then, the dynamics responses with different frequencies (0.1 Hz, 1.0 Hz and 4.0 Hz) are selected as experimental data for identification. Lastly, a Bayesian optimization based parameters identification approach is adopted to identify those unknown parameters [32, 33]. The identified parameters are listed in Table I. Fig. 6A-C shows the comparison between experimental data (used to identify the model) and model predicted results. The rest experimental data are used to further verify the identified model (such as Fig. 6D). The predicted errors are also illustrated in Fig. 7. It can be seen that the identified dynamic model can precisely describe the rate-dependent viscoelastic nonlinearity of the planar DEA under different

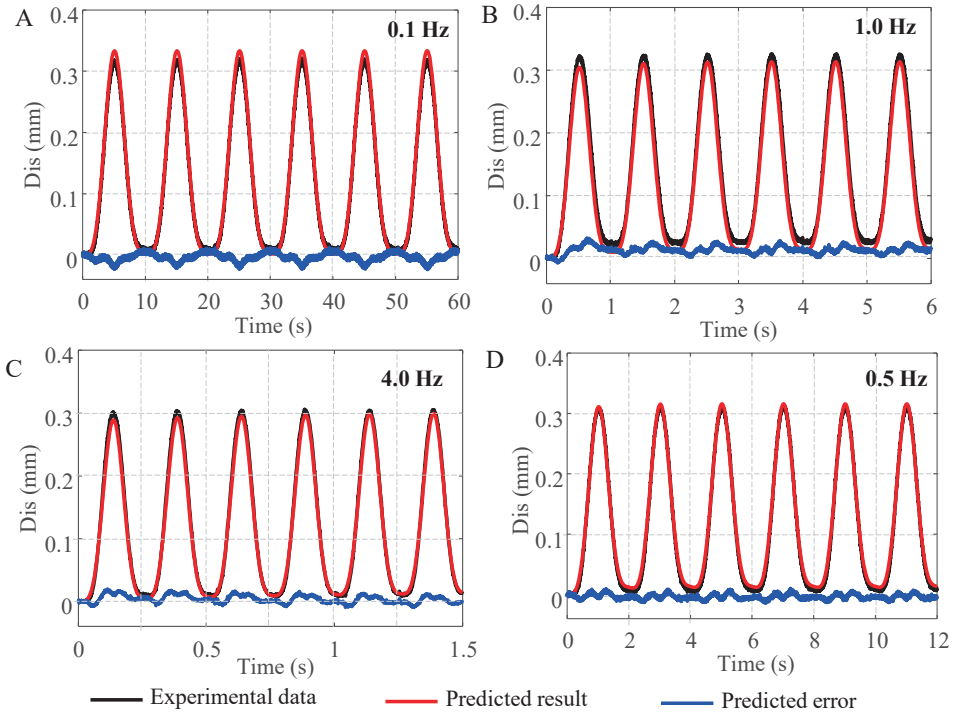

Figure 6. The comparison between the experimental data and predicted results under different frequencies. A-C) Experimental data with frequency of 0.1 Hz, 1.0 Hz and 4.0 Hz are used to identify the unknown parameters; D) One example of experimental data (0.5 Hz) are utilized to verify the effectiveness of the identified parameters.

frequency. To quantitatively characterize the predicted error, the max error e_m and root-mean-square error e_{rms} are defined as:

$$\begin{aligned} e_m &= \frac{\max|y_a - y_r|}{\max(y_r) - \min(y_r)} \times 100\%, \\ e_{rms} &= \frac{\sqrt{\frac{1}{N}\sum_{i=1}^{N}(y_a - y_r)^2}}{\max(y_r) - \min(y_r)} \times 100\%, \end{aligned} \tag{17}$$

where y_a and y_r represent the experimental data and predicted results, respectively, and N is the length of the y_a or y_r. Based on the definition, the e_m and e_{rms} listed in Table II are obtained from the dynamic model when the frequency is in the range of 0.1 Hz to 4.0 Hz.It clearly demonstrates the accuracy of the dynamic model and the e_m and e_{rms} are limited to 5% and 2% under different frequencies, respectively. Based on the dynamic model, we theoretically analyze the stability of the PBSMC. It demonstrates that when the λ, F, k_i, k_p and k_d are positive real, the PBSMC is stable (see more details in the Appendix A). To valid the effectiveness of the controller, we further conduct several experiments next.

Table 1. The identified parameters in the dynamic model.

Parameters	Value	Parameters	Value
k_1	570.825 (N/m)	η_1	0.077
k_2	129.208 (N/m)	η_2	0.225
k_3	4.417 (N/m)	η_3	3.448
k_3	0.162 (N/m)	η_4	17.101
b	0.0083	m	1.3 (g)
c	0.190	k	32.196 (N/m)
d	0.626	η_0	0.136

Table 2. The predicted errors with trajectories of different frequencies.

Fre/Hz	e_m/%	e_{rms}/%	Fre/Hz	e_m/%	e_{rms}/%
0.1	7.38	2.54	1.0	7.78	4.12
0.5	4.98	2.17	4.0	4.21	2.21

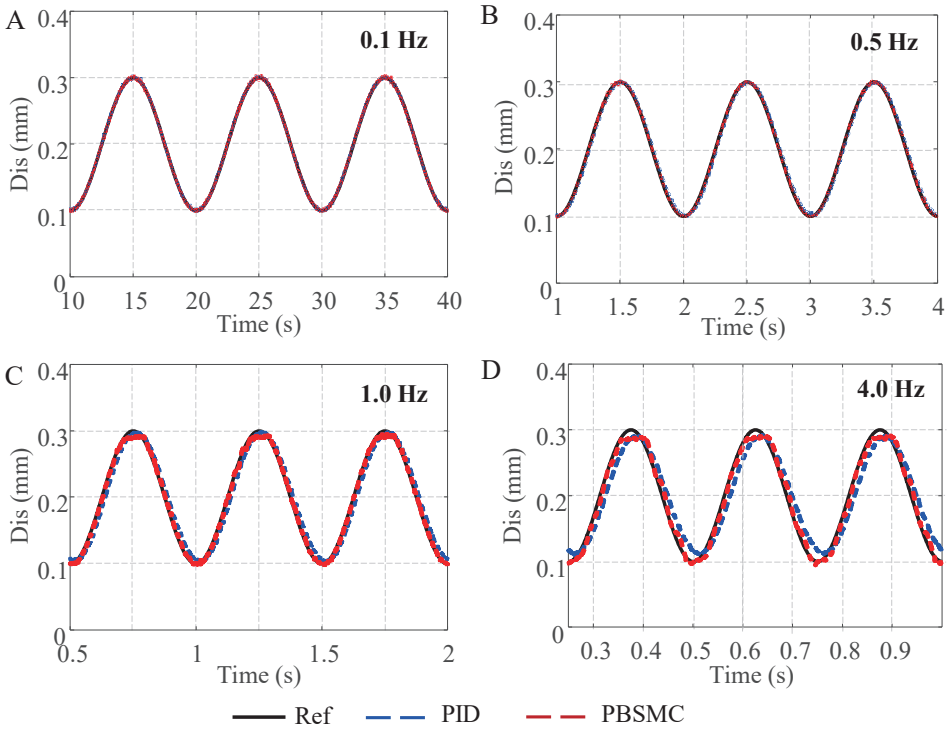

Figure 7. The comparisons of sinusoidal tracking experimental results with different controllers when the frequency equals to 0.1 Hz, 0.5 Hz, 1.0 Hz and 4.0 Hz, respectively.

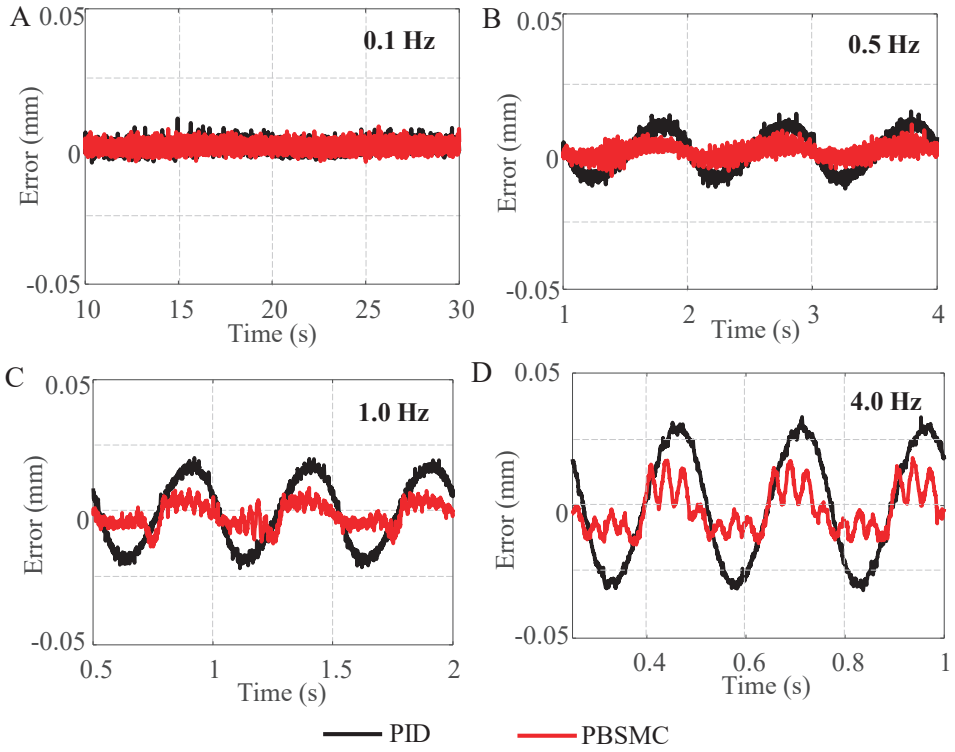

Figure 8. The comparison of tracking errors under different controllers when the frequency equals to 0.1 Hz, 0.5 Hz, 1.0 Hz and 4.0 Hz, respectively.

4. Experimental results

In this section, a series of trajectory tracking experiments are conducted to characterize the performance of the PBSMC. In addition, we adopted a PID controller for comparative experiments. Based on the stability condition, we firstly determine the λ, F, k_i, k_p and k_d for the PBSMC. Without loss of generality, λ, F, k_i, k_p and k_d are selected via a trial-and-error approach and the resulting values are 0.0001, 0.4, 220, 0.5 and 0.0001, respectively. For the PID controller, the k_i, k_p and k_d are selected as 50, 1.2 and 0.0001, respectively. Then, we investigate the tracking performance of the PBSMC and the PID controller by tracking different sinusoidal trajectories, when the frequency is in the range of 0.1 Hz to 4. 0 Hz. As an example, Fig. 7 shows the experimental results with the frequency of 0.1 Hz, 0.5 Hz, 1.0 Hz and 4.0 Hz. The corresponding tracking errors of the PBSMC and the PID controller are illustrated in Fig. 8. We can see that: with the PBSMC, the planar DEA can precisely track different sinusoidal trajectories while the PID controller is effective for the relative low frequency (such as 0.1 Hz in this work). Further, the output displacements are plotted as a function of reference displacement under different frequency (Fig. 9A for PBSMC and Fig. 9B for PID controller). The results clearly demonstrate that the PBSMC can remove the asymmetric and rate-dependent viscoelastic hysteresis nonlinearity (Fig. 3C). For the PID controller, there are obvious hysteresis loops that are still rate-dependent. The

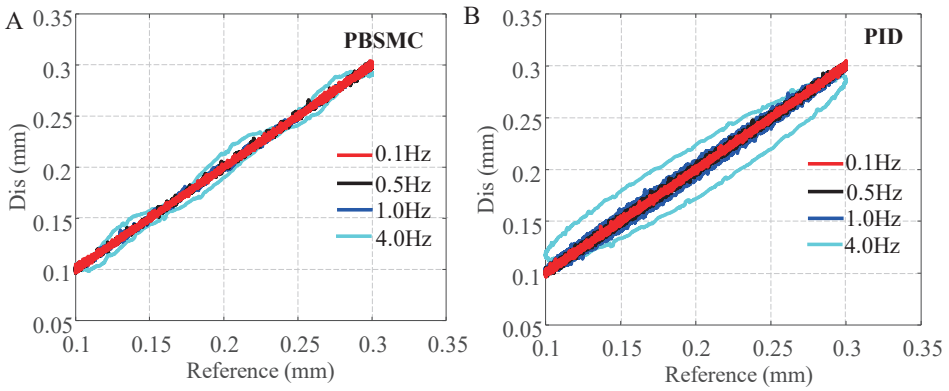

Figure 9. The comparison of hysteresis loops with different controllers.

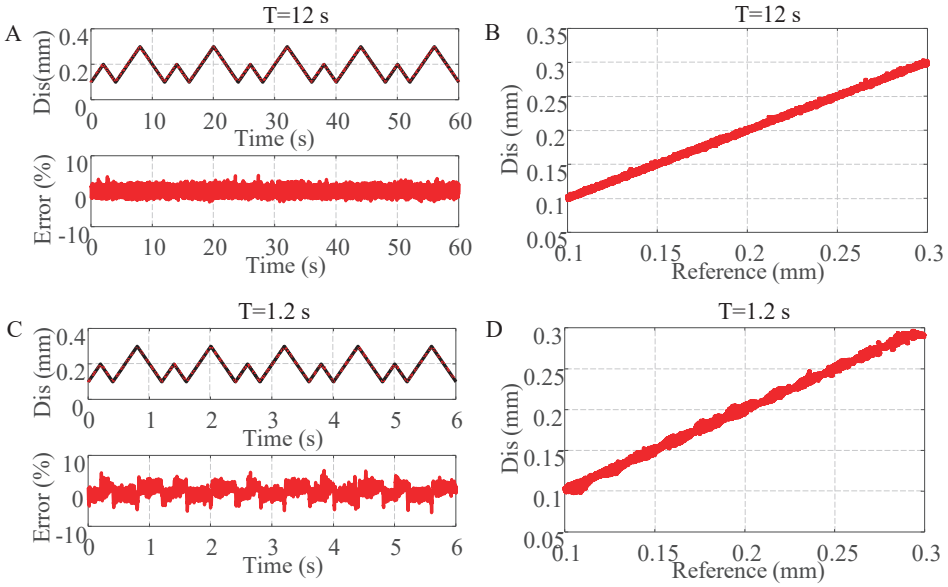

Figure 10. The experimental results of tracking different triangle trajectories.

main reason depends on the fact that the PID controller generally can not hand the viscoelastic hysteresis nonlinearity [19]. In addition, Table III lists the tracking errors with different control strategy. We can see that when the frequency is in a range of 0.1 Hz to 4.0 Hz, the PBSMC can reduce the e_m and e_{rms} from 45.87% and 24.46% to 8.72% to 3.88%, respectively, comparing with no controller. For the PID controller, it only can decrease the e_m and e_{rms} to 15.95% and 10.50%, respectively. Additionally, it should be noted that the amplitude of the displacement slowly decreases (Fig. 3B) when the frequency is in the range of 0.1 Hz to 4.0Hz. This indicates that the natural frequency of the planar DEA is very low (about few Hz), thereby limiting the working bandwidth of the PBSMC. As a result, the tracking errors also increase with increase in trajectory frequency (Fig. 6). Future work will focus on devising new methods aimed at improving the working bandwidth of the planar DEA.

In addition, the planar DEAs with the PBSMC can track different triangle

Table 3. The tracking errors with different controllers.

Controller	None		PID		PBSMC	
Fre/Hz	e_m/%	e_{rms}/%	e_m/%	e_{rms}/%	e_m/%	e_{rms}/%
0.1	36.26	22.73	4.25	0.62	3.55	0.56
0.5	37.21	23.11	5.76	1.75	4.26	0.86
1.0	34.30	19.81	7.12	3.43	4.81	1.24
4.0	45.87	24.46	15.95	10.50	8.72	3.88

trajectories with different period. For example, Fig. 10 shows the time domain output trajectory, tracking errors and hysteresis loops of experimental results when the period equals to 12 s and 1.2 s. We can see that the planar DEA can accurately track different triangle trajectories with e_m and e_{rms} of 6.08% and 1.59%, respectively, which further valid the effectiveness of the PBSMC.

5. Conclusions

In this work, we propose a new tracking control approach for DEAs by removing the rate-dependent viscoelastic hysteresis nonlinearity with PBSMC. To this end, we thoroughly investigate the viscoelastic nonlinearity of the planar DEA by the dynamic tests. The experimental results reveal the properties of the viscoelastic hysteresis nonlinearity, including rate-dependence and asymmetry. To remove this nonlinearity, the PBSMC is firstly formulated. Then, the stability of the controller is proved based on a dynamic model that can accurately describe the viscoelastic nonlinearity of the DEA. Lastly, different comparative tracking experiments are conducted to characterize the performance of the PBSMC. The experimental results demonstrate that with the PBSMC, the planar DEAs can precisely track a range of sinusoidal trajectories within a frequency range of 0.1 Hz and 4.0 Hz with the e_m and e_{rms} of 8.72% and 3.88%, respectively. Compared to open-loop trajectory tracking, the e_m and e_{rms} are decreased by 80.99% and 84.14%, verifying the effectiveness of the control approach.

The mechanism by which the PBSMC effectively suppresses the rate-dependent viscoelastic nonlinearity of DEAs is as follows: When PBSMC first acts on the DEA, it acts primarily as an extended sliding-mode controller for the initial stages of tracking, in order to bring DEA onto the sliding manifold of interest, as quickly as possible. This has the effect of eliminating the large force effects of the rate-dependent hysteresis. Once this occurs and DEA dynamics are on the manifold of interest, the extended PID part of PBSMC acts to reduce the relatively small position errors that occur due to the general viscoelastic nonlinearity of DEA.

As detailed earlier, although some interesting control approaches have been proposed to eliminate the nonlinearity of DEAs, most of them rely on dynamic

models which remain elusive for DEAs with the rate-dependent viscoelastic nonlinearity. Moreover, these control approaches are effective within specific frequency ranges or small deformation; limiting their wider application. As a significant improvement over these control schemes, our control approach provides a model-free control method to minimize rate-dependent viscoelastic nonlinearity of DEAs. The main advantages of the method reported in this paper are i) it eliminates the necessity for establishing a dynamic model for DEAs C a significantly difficult task and ii) it is independent of the geometry and electrode configuration of the DEAs. Consequently, our control approach can be easily be extended to other DEAs with wide applications.

Acknowledgement

This work was partially supported by the State Key Laboratory of Mechanical Transmissions (SKLMT-ZDKFKT-202004) and the National Natural Science Foundation of China (52005322).

References

[1] Tongqing Lu, Cheng Ma, and Tiejun Wang. Mechanics of dielectric elastomer structures: A review. *Extreme Mechanics Letters*, 38:100752, 2020.

[2] Jun Zhang, Jun Sheng, Ciarn T ONeill, and et. al. Robotic artificial muscles: Current progress and future perspectives. *IEEE Transactions on Robotics*, 35(3):761–781, 2019.

[3] Ron Pelrine, Roy Kornbluh, Qibing Pei, and et. al. High-speed electrically actuated elastomers with strain greater than 100%. *Science*, 287(5454):836–839, 2000.

[4] Lijuan Yin, Yu Zhao, Jing Zhu, and et. al. Soft, tough, and fast polyacrylate dielectric elastomer for non-magnetic motor. *Nature Communications*, 12(1):1–10, 2021.

[5] Guoying Gu, Jian Zhu, Limin Zhu, and et. al. A survey on dielectric elastomer actuators for soft robots. *Bioinspiration & biomimetics*, 12(1):011003, 2017.

[6] Ehsan Hajiesmaili and David R Clarke. Dielectric elastomer actuators. *Journal of Applied Physics*, 129(15):151102, 2021.

[7] Guoying Gu, Jiang Zou, Ruike Zhao, and et. al. Soft wall-climbing robots. *Science Robotics*, 3(25):eaat2874, 2018.

[8] Guorui Li, Xiangping Chen, Fanghao Zhou, and et. al. Self-powered soft robot in the mariana trench. *Nature*, 591(7848):66–71, 2021.

[9] Yufeng Chen, Huichan Zhao, Jie Mao, and et. al. Controlled flight of a microrobot powered by soft artificial muscles. *Nature*, 575(7782):324–329, 2019.

[10] Jun Shintake, Samuel Rosset, Bryan Schubert, Dario Floreano, and Herbert Shea. Versatile soft grippers with intrinsic electroadhesion based on multifunctional polymer actuators. *Advanced materials*, 28(2):231–238, 2016.

[11] Xiaobin Ji, Xinchang Liu, Vito Cacucciolo, and et. al. An autonomous untethered fast soft robotic insect driven by low-voltage dielectric elastomer actuators. *Science Robotics*, 4(37):eaaz6451, 2019.

[12] Liang Xu, Hanqing Chen, Jiang Zou, Wanting Dong, Guoying Gu, Limin Zhu, and Xiangyang Zhu. Bio-inspired annelid robot: a dielectric elastomer actuated soft robot. *Bioinspiration & Biomimetics*, 12(2):025003, 2017.

[13] Huichan Zhao, Aftab M. Hussain, Ali Israr, Daniel M. Vogt, Mihai Duduta, David R. Clarke, and Robert J. Wood. A wearable soft haptic communicator based on dielectric elastomer actuators. *Soft Robotics*, 7(4):451–461, 2020.

[14] Guoying Gu, U Gupta, Jian Zhu, Limin Zhu, and Xiangyang Zhu. Modeling of viscoelastic electromechanical behavior in a soft dielectric elastomer actuator. *IEEE Transactions on Robotics*, 33(5):1263–1271, 2017.

[15] Jiang Zou and Guoying Gu. Feedforward control of the ratedependent viscoelastic hysteresis nonlinearity in dielectric elastomer actuators. *IEEE Robotics and Automation Letters*, 4(3):2340–2347, 2019.

[16] Junshi Zhang, Bo Li, Hualing Chen, and Qibing Pei. Dissipative performance of dielectric elastomers under various voltage waveforms. *Soft matter*, 12(8):2348–2356, 2016.

[17] Zhigang Suo, Xuanhe Zhao, and William H. Greene. A nonlinear field theory of deformable dielectrics. *Journal of the Mechanics and Physics of Solids*, 56(2):467–486, 2008.

[18] Junshi Zhang, Liling Tang, Bo Li, Yanjie Wang, and Hualing Chen. Modeling of the dynamic characteristic of viscoelastic dielectric elastomer actuators subject to different conditions of mechanical load. *Journal of Applied Physics*, 117(8):084902, 2015.

[19] Jiang Zou and Guoying Gu. High-precision tracking control of a soft dielectric elastomer actuator with inverse viscoelastic hysteresis compensation. *IEEE/ASME Transactions on Mechatronics*, 24(1):36–44, 2018.

[20] Peng Huang, Jundong Wu, Pan Zhang, Yawu Wang, and Chunyi Su. Dynamic modeling and tracking control for dielectric elastomer actuator with model predictive controller. *IEEE Transactions on Industrial Electronics*, 69(2):1819–1828, 2022.

[21] Gianluca Rizzello, David Naso, Alexander York, and Stefan Seelecke. Modeling, identification, and control of a dielectric electro-active polymer positioning system. *IEEE Transactions on Control Systems Technology*, 23(2):632–643, 2015.

[22] Jiang Zou and Guoying Gu. Dynamic modeling of dielectric elastomer actuators with a minimum energy structure. *Smart Materials and Structures*, 28(8):085039, 2019.

[23] Gianluca Rizzello, Pietro Serafino, David Naso, and Stefan Seelecke. Towards sensorless soft robotics: Self-sensing stiffness control of dielectric elastomer actuators. *IEEE Transactions on Robotics*, 36(1):174–188, 2019.

[24] Gianluca Rizzello, David Naso, Biagio Turchiano, and Stefan Seelecke. Robust position control of dielectric elastomer actuators based on lmi optimization. *IEEE Transactions on Control Systems Technology*, 24(6):1909 – 1921, 2016.

[25] Thorben Hoffstadt and Jurgen Maas. Adaptive sliding mode position control for dielectric elastomer actuators. *IEEE/ASME Transactions on Mechatronics*, 22(5):2241–2251, 2017.

[26] Dehui Qiu, Yu Chen, and Yuan Li. Adaptive rbf neural network sliding mode control for a deap linear actuator. *International Journal of Performability Engineering*, 13(4):400–408, 2017.

[27] Cao Jiawei, Liang Wenyu, Zhu Jian, and Ren Qinyuan. Control of a muscle-like soft actuator via a bioinspired approach. *Bioinspiration & Biomimetics*, 13(6):066005, 2018.

[28] Ryo Kikuuwe. Torque-bounded admittance control realized by a set-valued algebraic feedback. *IEEE Transactions on Robotics*, 35(5):1136–1149, 2019.

[29] Ryo Kikuuwe, Satoshi Yasukouchi, Hideo Fujimoto, and Motoji Yamamoto. Proxy-based sliding mode control: a safer extension of pid position control. *IEEE Transactions on Robotics*, 26(4):670–683, 2010.

[30] Guoying Gu, Limin Zhu, Chunyi Su, Han Ding, and Sergej Fatikow. Proxy-based sliding-mode tracking control of piezoelectric-actuated nanopositioning stages. *IEEE/ASME Transactions on Mechatronics*, 20(4):1956–1965, 2014.

[31] Jiang Zou and Guoying Gu. Modeling the viscoelastic hysteresis of dielectric elastomer actuators with a modified rate-dependent prandtlishlinskii model. *Polymers*, 10(5), 2018.

[32] Jasper Snoek, Hugo Larochelle, and Ryan P Adams. Practical bayesian optimization of machine learning algorithms. *Advances in neural information processing systems*, 25, 2012.

[33] Eric Brochu, Vlad M Cora, and Nando De Freitas. A tutorial on bayesian optimization of expensive cost functions, with application to active user modeling and hierarchical reinforcement learning. *arXiv preprint arXiv:1012.2599*, 2010.

Appendix A: stability analysis

To prove the stability of the PBSMC, we firstly define the following state variables:

$$z = [z_1, z_2, z_3, z_4, z_5, z_6] = [z_1, z_2, z_3, z_4, x, \dot{x}]\,. \tag{A.1}$$

Then, (15) can be rewritten as:

$$\begin{aligned}
\dot{z}_1 &= z_6 - \tfrac{k_1}{\eta_1} z_1,\\
\dot{z}_2 &= z_6 - \tfrac{k_2}{\eta_2} z_2,\\
\dot{z}_3 &= z_6 - \tfrac{k_3}{\eta_3} z_3,\\
\dot{z}_4 &= z_6 - \tfrac{k_4}{\eta_4} z_4,\\
\dot{z}_5 &= z_6,\\
\dot{z}_6 &= \tfrac{F(z_5,U)}{m} - \tfrac{\eta_0}{m} z_6 - \tfrac{k}{m} z_5 - \tfrac{1}{m}\sum_{i=1}^{4} k_i z_i,
\end{aligned} \tag{A.2}$$

and

$$F\left(z_5, U\right) = U^2\left(b z_5^2 + c z_5 + d\right). \tag{A.3}$$

It should be mentioned that $F\left(z_5, U\right)$ is replaced with f_{in} when put in closed-loop control. In addition, the goal of this work is to achieve high-precision tracking control of DEAs by removing the rate-dependent viscoelastic nonlinearity. To verify the effectiveness of the controller, sinusoidal waves with different frequencies are used as desired trajectories. Therefore, the desired trajectory, its first and second derivatives, respectively, can be expressed as:

$$r = A\sin\left(2\pi f t - \frac{\pi}{2}\right) + B, \tag{A.4}$$

$$\dot{r} = 2\pi f A\cos\left(2\pi f t - \frac{\pi}{2}\right), \tag{A.5}$$

$$\ddot{r} = -4\pi^2 f^2 A\sin\left(2\pi f t - \frac{\pi}{2}\right), \tag{A.6}$$

where A, B, f and t represent the amplitude, offset, frequency and time of the desired trajectory, respectively. The error dynamics of (A.1) can be determined as follows:

$$e = r - z_5, \tag{A.7}$$

Next, its first and second derivatives are defined as

$$\begin{aligned}
\dot{e} &= \dot{r} - z_6,\\
\ddot{e} &= \ddot{r} - \dot{z}_6,
\end{aligned} \tag{A.8}$$

Substituting (A.7-A.8) into (A.2), we can obtain

$$m\ddot{e} + \eta_0\dot{e} + ke = -f_{in} + \varphi, \tag{A.9}$$

where

$$\varphi \triangleq m\ddot{r} + \eta_0\dot{r} + kr + \sum_{i=1}^{4} k_i z_i. \tag{A.10}$$

In order to prove the stability of the PBSMC in this work, the method in [30, 31] are used to formulate the stability analysis. Given that $\|r\|$ is upper bounded and since it is the desired trajectory, $\|\dot{r}\|$ and $\|\ddot{r}\|$ are also bounded. As a result, the φ must be bounded

$$\left\{\|\varphi\| \leq \varepsilon_0, \varepsilon_0 \in R^+\right\}. \tag{A.11}$$

Thus, there exists a positive definite function proving stability of the closed-loop system. In order to prove the stability of the overall controller, firstly consider the stability of the sliding mode control portion that can be expressed as:

$$\dot{z}_5^p = z_6^p, \tag{A.12}$$

$$\dot{z}_6^p = -\frac{F_{PID}}{m_p} + F_{eq}, \tag{A.13}$$

where z_5^p and z_6^p represent the x_p and $\dot{x}_p$ in (2). F_{eq} is the equivalent control input for the proxy mass that consists of the inverting input F_{inv} and the switching law F_{SMC}:

$$F_{eq} = F_{inv} + F_{SMC}. \tag{A.14}$$

To obtain F_{inv} and for derivation purpose, F_{SMC} is set as zero as F_{SMC} is purely for keeping the system on the desired trajectory once reaching phase of the sliding-mode control is over, in short $F_{eq} = F_{inv}$. Begin by differentiating:

$$\dot{\sigma}_1 = \dot{r} - z_6^p + \lambda\left(\ddot{r} - \dot{z}_6^p\right). \tag{A.15}$$

To impose the sliding condition in which tracking is achieved and hence solve for F_{inv}, consider $\dot{\sigma}_1 = 0$ and substitute (A.13) into (A.15) and equals to zero:

$$\dot{\sigma}_1 = \dot{r} - z_6^p + \lambda\left(\ddot{r} + \frac{F_{PID}}{m_p} - F_{inv}\right) = 0. \tag{A.16}$$

Thus

$$F_{inv} = \frac{\dot{r} - z_6^p}{\lambda} + \ddot{r} + \frac{F_{PID}}{m_p}. \tag{A.17}$$

Therefore, the combined control input to provide tracking and staying on the sliding surface is given as:

$$F_{eq} = \overbrace{\frac{\dot{r} - z_6^p}{\lambda} + \ddot{r} + \frac{F_{PID}}{m_p}}^{F_{inv}} + \overbrace{F\mathrm{sgn}\left(\sigma_1\right)}^{F_{SMC}}. \tag{A.18}$$

To prove the stability of the sliding-mode control of the proxy mass, we define $Z = [z_5^p, z_6^p] \in R^2$ and select the Lyapunov function as:

$$V\left(Z\right) = \frac{1}{2}\sigma_1^2. \tag{A.19}$$

Such a function satisfies the following conditions of: $V(Z) = 0$ iff $Z = 0$, $V(Z) > 0$ iff $Z \neq 0$. By differentiating (A.19) with respect to time:

$$\dot{V}\left(Z\right) = \sigma_1\dot{\sigma}_1. \tag{A.20}$$

Here, (A.18) is substituted into (A.13) which is then resubstituted into (A.15). When expanding and cancelling terms, this leaves:

$$\dot{\sigma}_1 = -\lambda F \mathrm{sgn}\left(\sigma_1\right). \tag{A.21}$$

Then, substitute (A.21) into (A.20):

$$\dot{V}\left(Z\right) = -\sigma_1 \lambda F \mathrm{sgn}\left(\sigma_1\right) = -\lambda F \left\|\sigma_1\right\|. \tag{A.22}$$

We should note that $\sigma_1 \mathrm{sgn}\left(\sigma_1\right) \equiv \left\|\sigma_1\right\|$ is used here. For closed-loop stability, $\dot{V}\left(Z\right) \leq 0$ is required. Providing $\{F \in R, F > 0\}$ and $\{\lambda \in R, \lambda > 0\}$, this satisfies the condition $\dot{V}\left(Z\right) \leq 0$ and $\dot{V}\left(Z\right) < 0 \forall Z \neq 0$, thereby providing stability of the SMC on the proxy mass equations. This leaves providing the stability of the PID portion of the closed-loop system. It should be mentioned that the stability of the PID controller relies on the stability derivation for the sliding mode control just derived. The error dynamic model (A.9) can be used to prove the conditions necessary for stability. Let following system of equations based (A.9) be defined along with extra states for the PID controller:

$$\begin{aligned}
&\dot{p}_1 = p_2, \\
&\dot{p}_2 = \tfrac{1}{m}\left[\varphi - f_{in}\left(p_3, p_4, p_5\right) - \eta_0 p_2 - k p_1\right], \\
&\dot{p}_3 = \dot{a}, \\
&\dot{p}_4 = \ddot{p}_3, \\
&\dot{p}_5 = \ddot{p}_4, \\
&f_{in} = k_i p_3 + k_p p_4 + k_d p_5.
\end{aligned} \tag{A.23}$$

Then, we define a Lyapunov function as:

$$V_p\left(P\right) = \frac{1}{2}\left(k p_1^2 + m p_2^2\right). \tag{A.24}$$

By differentiating (A.24), we can get:

$$\dot{V}_p\left(P\right) = k p_1 \dot{p}_1 + m p_2 \dot{p}_2. \tag{A.25}$$

Substitute (A.23) into (A.25):

$$\dot{V}_p\left(p\right) = -\eta_0 p_2^2 + \left[\varphi - \left(k_i p_3 + k_p p_4 + k_d p_5\right)\right] p_2. \tag{A.26}$$

Based on (A.26), if the $\dot{V}_p\left(P\right) \leq 0$, the $\varphi - \left(k_i p_3 + k_p p_4 + k_d p_5\right) \leq 0$ has to be satisfied. Considering φ is upper bounded by the constant ε_0 and the PID state variables p_3, p_4 and p_5 must be bounded, the condition of $\varphi - \left(k_i p_3 + k_p p_4 + k_d p_5\right) \leq 0$ can be equivalent to:

$$\left\|\varphi\right\| - \left(k_i \left\|p_3\right\| + k_p \left\|p_4\right\| + k_d \left\|p_5\right\|\right) < 0. \tag{A.27}$$

It can be seen, if $k_i > 0$, $k_p > 0$ and $k_d > 0$, the $\dot{V}_p\left(P\right) \leq 0$. Combing with (A.22) and (A.27), it demonstrates that when the λ, F, k_i, k_p and k_d are positive real, the PBSMC is stable.